Российская Академия Наук

РОССИЙСКАЯ АКАДЕМИЯ НАУК

ИНСТИТУТ ПРОБЛЕМ БЕЗОПАСНОГО РАЗВИТИЯ АТОМНОЙ ЭНЕРГЕТИКИ

ИБРАЭ

RUSSIAN ACADEMY OF SCIENCES

NUCLEAR SAFETY INSTITUTE

Препринт ИБРАЭ № IBRAE-2002-14

Preprint IBRAE-2002-14

A. V. Berdyshev, M. S. Veshchunov

MODELLING OF GRAIN FACE DIFFUSION TRANSPORT AND SWELLING IN UO_2 FUEL

Москва
2002

Moscow
2002

Бердышев А.В., Вещунов М.С. МОДЕЛИРОВАНИЕ ДИФФУЗИОННОГО ПЕРЕНОСА ПРОДУКТОВ ДЕЛЕНИЯ ПО ПОВЕРХНОСТЯМ ЗЕРЕН И РАСПУХАНИЯ В ТОПЛИВЕ UO_2. Препринт № IBRAE-2002-14. Москва: Институт проблем безопасного развития атомной энергетики РАН, 2002. 19 с. — Библиогр.: 29 назв.

Аннотация

Разработана модель переноса продуктов деления по поверхностям зерен, самосогласованно учитывающая процесс поверхностной диффузии газовых атомов, а также процессы их стекания в зернограничные пузыри и перерастворения. Выделено важное влияние зернограничной диффузии газовых атомов на выход продуктов деления до образования открытой пористости. В качестве главного механизма релаксации пузырей на гранях зерен топлива рассматривается процесс коалесценции пузырей. Получено удовлетворительное согласие результатов численных расчетов по коду MFPR с новыми моделями и различными доступными экспериментальными данными по выходу продуктов деления из облученного топлива, распуханию топлива и микроструктуре поверхностей зерен.

©ИБРАЭ РАН, 2002

Berdyshev A.V., Veshchunov M.S. MODELLING OF GRAIN FACE DIFFUSION TRANSPORT AND SWELLING IN UO_2 FUEL. Preprint IBRAE-2002-14. Moscow: Nuclear Safety Institute RAS, June 2002. 19 p. — Refs.: 29 items.

Abstract

An advanced model for the grain face transport based on the self-consistent consideration of gas atoms diffusion, sinking to and resolution from bubbles on grain faces, is developed. An important role of grain boundary diffusion of gas atoms to edges before interlinking of inter-granular bubbles, is outlined. The coalescence of face bubbles due to their random migration is considered as the main mechanism of grain face bubbles relaxation. Implementation in the MFPR code of the new model and numerical treatment of various available data on gas release from irradiated fuel, fuel swelling and grain face microstructure, show a satisfactory agreement of the code predictions with measurements.

©Nuclear Safety Institute, 2002

Modelling of grain face diffusion transport and swelling in UO_2 fuel

A.V. Berdyshev and M.S. Veshchunov

Nuclear Safety Institute (IBRAE), Russian Academy of Sciences

B.Tul'skaya, 52, Moscow, 113191

phone: (095) 955 2218, fax: (095) 958 0040, e-mail: vms@ibrae.ac.ru

Content

1 Introduction 3
2 Model for fission gas diffusion transport on grain faces 3
2.1 Model description 5
2.1.1 Extra-granular porosity geometry 5
2.1.2 Basic equations 6
2.2 Model implementation in MFPR code 7
2.3 Model validation 8
3 Model for grain face porosity evolution 10
3.1 Analysis of experimental observations 10
3.2 Model development and validation 10
4 Conclusions 12
Acknowledgements 13
References 14
Figures 15

1 Introduction

In a recent paper on the theory of fission gas bubble evolution in irradiated UO_2 fuel [1] it was demonstrated that currently existing models and codes generally underestimate irradiation effects at temperatures below 1500°C and thermal effects at temperatures above 1500°C. In order to improve the microscopic description of the fission gas behaviour, new models were developed and implemented in the mechanistic code MFPR (Module for Fission Product Release) that is currently under development in collaboration between IBRAE (Moscow) and IRSN (Cadarache, France) [2].

This allowed a significant improvement of the code predictions with respect to gas release and fuel swelling under various conditions of UO_2 fuel operation: steady-state irradiation, transient and post-irradiation annealing. The description of the newly developed models, their implementation in the MFPR code and some results of the code validation, were presented in [3].

In the present paper further development and improvement of the model for the grain face diffusion transport and porosity evolution, is presented. In Section 2 the model for fission gas diffusion transport to grain edges accompanied with absorption by and resolution from inter-granular bubbles, is considered. In Section 3 the model is extended to consideration of grain face porosity evolution due to grain face bubbles coalescence. Validation of the new model against various tests from the literature including either integral (release and swelling) or microscopic measurements (bubble size and density on grain surface) at different temperatures, fission rates and burn-ups, is also presented in the following Sections.

2 Model for fission gas diffusion transport on grain faces

In the majority of the currently existing models for gas release from UO_2 fuel, it is assumed that during steady-state reactor operation the grain boundary bubbles increase in size and number until they touch, allowing gas release to the fuel/clad gap [4–7]. The grain boundary bubbles appear to be relatively immobile, particularly at temperatures below about 1900 K [8], and it is usually assumed that gas release occurs only on interlinking. The time for the "grain-face porosity saturation" to occur corresponds with an incubation time period of bubble growth [5]. It is generally accepted now that the grain face porosity saturates at the fractional coverage of the grain boundaries occupied by bubbles ≈ 50%, and commencement of gas release from grain faces to edges (and further through the edge tunnels outside the grain) is usually associated with the formation of the open porosity network at this coverage [4–7].

However, in recent tests [9, 10] this conclusion on the commencement of gas release was not confirmed. In these tests the 3 and 4 BWR cycle specimens with ≈ 2.4 and 2.9% burnup, respectively, were taken from the outer pellet region (between rim and middle), and the fractional coverage of grain faces by bubbles was evaluated from SEM photographs as ≈ 6 and 10% [10], respectively, see Fig. 1. Despite such low values of the grain face coverage, significant fractional fission gas release (up to 20–30%) during their base irradiation was measured by pin puncture tests from these specimens, Fig. 2. Therefore, a noticeable gas release from these fuel samples occurred at a coverage far below the saturation value ≈ 50% and without visible bubble interlinking on the grain faces. The irradiation temperature at the location of the specimens was not directly measured, but might be evaluated as 1150–1250°C from their maximum linear heat generation rates (between 300 and 370 W/cm).

On the other hand, a significant burst release observed in these tests during post-irradiation annealing at 1600–1800°C was invariably associated in [9, 10] with the coverage of about 40–50% attained under various burnups and heating conditions, Fig. 3. Hence, interlinking of grain face bubbles at the threshold value of the coverage ≈ 50% considered in the models [4–7] might be responsible for the secondary burst release observed in the annealing stage of the tests [9, 10].

Therefore, from these tests it can be generally concluded that at low irradiation temperatures (1250°C) the formation of the open porosity network can be significantly delayed, but this does not prevent the commencement of gas release. Indeed, 4 irradiation cycles were insufficient for the attainment of the saturation coverage, whereas gas release was significant (20–30%) at a rather low coverage 6–10%.

To avoid this contradiction, one should additionally consider an input in the total gas release of the diffusion transport of gas atoms along grain faces in presence of grain boundary traps (bubbles). This diffusion transport becomes dominant in the lack of interlinking of grain face bubbles. Usually the diffusion process is considered only in evaluation of the grain face bubble size [11–14] and/or estimation of the incubation period for saturation coverage [4, 5], since it is assumed that practically all the gas diffused from grains to grain boundaries is collected by the growing grain face bubbles and only a negligible part is transported to grain edges (before interlinking of grain bubbles). This assumption was seemingly supported by the theoretical paper [14] where it was shown that the sink strength of the grain face periphery (edges) becomes (after some initial time interval) negligibly small in comparison with the total sink strength of the growing grain face bubbles. A similar conclusion was recently derived in [15]. However, as will be shown below, this conclusion can be strongly violated if one additionally considers re-solution of gas atoms from face bubbles back to the grain matrix (not considered in [14]), that may essentially redistribute the outcoming diffusion flux from grains among different sinks on grain faces.

Indeed, as shown in [16] re-dissolved atoms are knocked some distance δ into the grain from the grain boundary, whence they may proceed to diffuse again. The built-up concentration barrier c_δ of the resolution layer reduces the diffusion flux from the grain J_{dif}, on the one hand, and determines the net flux of atoms deposited on the grain boundary $J_\delta \approx Dc_\delta/\delta$, on the other hand [16]. This flux J_δ should counterbalance the resolution flux back into the grain J_{res} and, in accordance with the flux matches $J_{dif} + J_{res} = J_\delta$ (see below), may essentially exceed the "source term" from the grain J_{dif}. Namely this flux J_δ should be redistributed among various grain face sinks (bubbles and edges) rather than the source term flux J_{dif}. Neglecting such an effect, the author [14] underestimated the grain boundary diffusion flux to edges.

On the other hand, such a process of gas atom resolution from grain faces was considered in other papers (say, [4, 11, 16]), however, in these papers the grain face diffusion transport to edges was not included in consideration.

In a recent paper [17] simultaneous consideration of various processes on grain faces (atom diffusion, trapping by and re-solution from the grain boundary bubbles) was proposed in order to reconcile various approaches, and a model formally analogous to one presented in the current paper was formulated for the first time. However, some simplifications of the model adopted for numerical analysis of coupled equations for intra- and inter-granular transport apparently prevented the author [17] from important conclusions of the present paper concerning essential role of atomic grain face transport to edges in the course of face bubbles growth. For this reason, in the subsequent paper [15] the author concluded that the contribution of grain boundary diffusion to fission gas release on the pellet scale is strongly inhibited as soon as the aerial coverage of the grain boundary traps is about 1% , and consequently a simplified or alternative model for the inter-granular behaviour of fission products was further developed.

In the present paper an essential role of the grain face diffusion transport in the gas release mechanism is highlighted, in order to explain the above mentioned [9, 10] and some other observations. For this purpose a completely self-consistent scheme for analysis of diffusion and re-solution processes in the grain and grain faces is considered.

In particular, it is shown that "circulation" of gas atoms collected by growing intergranular bubbles from the grain face and then returned back (by the resolution process) into the grain matrix, makes bubbles much less effective sinks for gas atoms in the course of their growth saturation (i.e. approaching a balance among absorbed and re-emitted atoms) and thus continuously increases a fraction of the source term flux J_{dif} (from grain bulk) eventually transported to edges. Specifically, this leads to a natural conclusion that in the limiting case of the complete balance (among absorbed and re-emitted atoms) and cessation of the face bubble growth (before their interlinking), 100% of the source term flux will be transported to grain edges via grain face diffusion process.

Implementation in the MFPR code of the improved model of the grain face and numerical treatment with the new model of various available data on grain face microstructure and gas release from irradiated fuel, allow a satisfactory agreement with measurements. An important possible application of the model to the MOX fuel is additionally emphasised.

2.1 Model description

2.1.1 Extra-granular porosity geometry

The development of the gas release model for FP release out of grain interior is considerably simplified by an assumption of spherical grains UO_2. However, an accurate treatment of extra-granular porosity requires more adequate UO_2 grain shape specification. In a more realistic approach the shape of UO_2 grains is considered as truncated octahedron or tetrakaidecahedron (TDK) [4]. The TDK has 14 faces, six of which are square and eight hexagonal, 36 edges and 24 corners. When packed together an array of TDKs can fill all available space in a solid and thus represents an appropriate basic building block. The meeting point of each grain face is shared by two grains, each grain edge by three grains and each grain corner by four grains. Hence, on average each grain has $N_{fpgr} = 7$ faces, $N_{epgr} = 12$ edges and $N_{cpgr} = 6$ corners.

The volume of various bubbles is calculated by multiplication of the volume of a sphere with the same curvature radius by a correction factor, which depends on the semidihedral angle θ:

$$V_i = \frac{4}{3}\pi R_i^3 f_i(\theta). \tag{1}$$

Grain face lenticular bubbles are formed by intersection of two spherical surfaces and hence have a circular projection. The projected circular radius is $R_f \sin\theta$, the correction factor for the volume is [20]

$$f_f(\theta) = 1 - \frac{3}{2}k + \frac{k^2}{2}, \tag{2}$$

where $k = \cos\theta$.

Cigar-shaped edge bubbles are formed by intersection of three spherical surfaces. The length of an edge bubble is connected with its radius of curvature by the relationship:

$$l_e = 2R_e\sqrt{1 - \frac{4k^2}{3}}, \tag{3}$$

and the volume correction factor is

$$f_e = \frac{3}{2\pi}\left[\pi - 2\alpha + \frac{k^2}{3}\sqrt{3 - 4k^2} - \beta k\left(3 - k^2\right)\right], \tag{4}$$

where

$$\alpha = \arcsin\left(\frac{1}{2\sqrt{1-k^2}}\right), \qquad \beta = \arccos\left(\frac{k}{\sqrt{3(1-k^2)}}\right).$$

Grain corner bubbles are constructed by intersection of four spherical surfaces and in shape are close to the spherical ones. For the simplicity, in the MFPR code these corner bubbles are assumed to have a spherical form.

2.1.2 Basic equations

Owing to an extremely high ratio of the gas atom diffusion coefficients on grain faces D_f and in the grain matrix D_g, which is usually believed to be of the same order of magnitude as that for the uranium self-diffusion coefficients, $D_f/D_g \sim 10^5$ [18], one can apply results of the steady-state consideration of the grain face diffusion problem [14] to calculate the face bubbles and edges sink strengths in the mean field approximation:

$$(k_e R_{gf})^2 = 2k_b R_{gf} I_1(k_b R_{gf})/I_2(k_b R_{gf}), \tag{5}$$

where k_e^2 and k_b^2 are the total sink strengths of the grain face edges and bubbles; I_1 and I_2 represent the first and the second modified Bessel functions of the first kind, respectively; R_{gf} is the grain face radius.

The corrected expression for the bubbles sink strength in a cellular model in which each face bubble with a mean radius R_f in the plane of the grain boundary is surrounded by a concentric sink-free region with radius R_s [14], takes the form:

$$(k_b R_s)^2 = 8(1-\varphi)^2/[(1-\varphi)(\varphi-3) - 2\ln\varphi], \tag{6}$$

where $\varphi = (R_f/R_s)^2$ is the grain face coverage.

In such a (mean field) approximation, if fission gas is deposited uniformly at some rate $2J_\delta$ atoms per unit area on each grain face from two adjacent grains, $2J_\delta\varphi$ goes directly to face bubbles. The flow distribution of the remainder between the face bubbles J_f and edges J_e may be described by the following equations:

$$J_f = k_b^2 D_f \tilde{c}\ \pi R_{gf}^2, \tag{7}$$

and

$$J_e = k_e^2 D_f \tilde{c}\ \pi R_{gf}^2, \tag{8}$$

where $\tilde{c}$ is the mean concentration of gas atoms dissolved in the grain boundary, which can be calculated from the steady-state balance equation:

$$2J_\delta(1-\varphi) = (k_e^2 + k_b^2) D_f \tilde{c}\ . \tag{9}$$

As above explained, the deposition rate J_δ cannot be equated to the diffusion source term J_{dif} from the grains, since gas atoms re-emitted from the face bubbles to the grains (in some resolution layer with the thickness δ around the grain face) will tend to return back to the grain face sink, thus increasing the net flux onto the grain face. This flux J_δ has to counterbalance the resolution flux back into the grains J_{res} and thus obeys the flux matches in the vicinity δ of the grain boundary:

$$J_{dif} + J_{res} = J_\delta. \tag{10}$$

Therefore, the calculation of the deposited flux also requires evaluation of the resolution flux J_{res} from the grain face.

Usually the resolution flux J_{res} (into each of two adjacent grains) is evaluated as $b_v N_f/2$, where b_v is the resolution probability and N_f is the number of atoms per unit area of the grain face [4–7], i.e. by smearing over the grain face surface structure. For this reason, the resolution flux does not depend on the amount and size of face bubbles, but depends only on the total amount of gas atoms in the bubbles. Such a consideration significantly simplifies the resolution process modelling, however, prevents from correct description of the grain face diffusion fluxes redistribution among various surface sinks.

Indeed, since gas atoms are deposited over the whole grain face area (unoccupied and covered by bubbles), but are emitted into the grains from the face bubbles, some "circulation" of gas atoms (coming from and returning back into the grains) through the grain face bubbles occurs. The emission rate increases with the bubble size growth, thus, for instance, under certain conditions may completely counterbalance the absorption rate, leading to the cessation of the grain face bubbles growth. Under such conditions the absorbed by bubbles part of the deposited flux J_δ will be completely returned back to the grains by the resolution flux J_{res}, therefore, the source term flux J_{dif} will be completely transported to the grain edges. Under more general conditions of continuously growing bubbles (up to their interlinking) the gas atoms absorption will be compensated by the resolution process only partially, thus reducing the flux J_e to the edges. However, in all the cases this flux J_e will be significantly higher than one calculated in neglect of the above described circulation process.

To calculate the resolution flux J_{res}, one should also take into account that according to the Nelson's model [21] for intra-granular bubbles, the resolution rate is independent of the bubble size only for very small bubbles ($R_b \leq$ 1–1.5 nm). For larger spherical bubbles only a fraction of gas atoms within a critical distance from the

bubble surface $\lambda \approx 1$–1.5 nm may be escaped, therefore, the resolution rate becomes inversely proportional to the bubble radius, $b_0 N_b (\lambda/R_b)$, where b_0 is the resolution probability and N_b is the number of atoms in a bubble. Despite the grain face bubbles have a more complicated form, this conclusion can be generalised also for lenticular bubbles with a radius R_f in the plane of the grain boundary, probably, with some renormalisation of the resolution parameters b_0 and λ. A similar procedure can be applied to resolution from grain edge and corner bubbles. In the following calculations, for simplicity the same values of these parameters as for the spherical bubbles, will be used, i.e. $\lambda \approx 1$–1.5 nm [21] and $b_0 \approx (2–3)\cdot 10^{-17}$ cm^3 [22, 1]. Correspondingly, the resolution flux takes the form:

$$J_{res} = \omega_{rsi}^{f} N_f + \omega_{rsi}^{e} N_e + \omega_{rsi}^{c} N_c, \tag{11}$$

where $\omega_{rsi}^{f(e,c)} = b_0\lambda/(\lambda + R_{f(e,c)})$ is the irradiation-induced resolution rate of atoms from face (edge, corner) bubbles, respectively; $N_{f(e,c)}$ is the average number of atoms in a face (edge, corner) bubble, respectively.

Eqs. (10) and (11) determine the mean gas atom concentration $\tilde{c}$ in the grain face by their substitution in the balance Eq. (9):

$$2\,(J_{dif} + J_{res})\,(1 - \varphi) = (k_e^2 + k_b^2) D_f \tilde{c}\ . \tag{12}$$

The source term flux J_{dif} entering in Eq. (12), should be self-consistently calculated with the new boundary condition $c = c_\delta$ at the resolution layer boundary δ, as recommended by Turnbull [11].
The competition between the absorption and resolution processes determines the growth rate of a bubble:

$$\mathrm{d}N_f/\mathrm{d}t = k_b^2 \pi R_s^2 D_f\ \tilde{c} + 2J_\delta \pi R_f^2 - \omega_{rsi}^{f} N_f. \tag{13}$$

The volume of a grain face lenticular bubble is calculated by Eqs. (1) and (2).

Under assumption that the pressure P inside the bubble balances the capillary forces restraining the bubble in addition to any external pressure P_{ext}, and using the ideal gas law (valid for relatively large grain face bubbles with $R_f > 5$ nm), one gets

$$N_f = PV_b/kT = (4\pi R_b^3/3kT)\, f_f(\theta)(P_{ext} + 2\gamma/R_f), \tag{14}$$

where γ is the free surface energy (e.g. [4]).

The radius R_s of a concentric sink-free region around each face bubble is determined by the mean number density X_f of bubbles on a grain face, $R_s \approx (\pi X_f)^{-1/2}$, which was visually analysed in several independent tests, e.g. [10, 23, 24]. In all these observations the bubble number density varied in the range $X_f \approx 10^{11}$–10^{13} m^{-2} and might be fairly well approximated in a wide temperature interval 800–1900°C by the formula:

$$X_f = 3.67\cdot 10^8 \cdot \exp(1.314\cdot 10^4/T)\ \mathrm{m}^{-2}, \tag{15}$$

where T is in K. At low temperatures the concentration was limited by the value of 10^{13} m^{-2}.

2.2 Model implementation in MFPR code

An equation for volume concentration of gas atoms in grain face babbles, Y_f, can be obtained by multiplication of both parts of Eq. (13) by C_f (where $C_f = X_f \cdot 3/d_{gr}$ is the volume concentration of face bubbles) and substitution of Eqs. (10)–(12):

$$\begin{aligned} \frac{d}{dt} Y_f &= (F_{gr\to f} + F_{res}) - (F_{gr\to f} + F_{res})(1-\phi)\frac{k_e^2}{k_b^2 + k_e^2} - \omega_{rsi}^{f} Y_f \\ &= F_\delta - F_{f\to e,c} - F_{f\to gr} \end{aligned} \tag{16}$$

where $F_{gr\to f}$ is volume density of overall flux of xenon atoms out of fuel grains including the diffusion and biased migration fluxes of gas atoms and bubbles, fluxes due to grain boundary sweeping, etc. Fluxes F_i introduced in Eq. (16) are related to the unit of fuel volume. They are connected with surface flux densities J_i, through the surface to volume ratio of the fuel grains $S/V = 3/d_{gr}$, i.e. $F_i = (3/d_{gr})J_i$.

The first term in the r.h.s. of Eq. (16), F_δ, describes the overall flux of xenon atoms deposited on grain boundaries, the second one, $F_{f\to e,c}$, represents the flux of Xe atoms from grain faces to grain edges and corners, the last one, $F_{f\to gr}$, is the resolution flux of Xe atoms from face bubbles into the grains.

The flux of xenon atoms from grain faces to their boundaries determines the formation rate of edge and corner bubbles:

$$\frac{d}{dt}Y_e = \eta_e F_{f\to e,c} - \omega_{rsi}^{e} Y_e, \tag{17}$$

$$\frac{d}{dt}Y_c = \eta_c F_{f\to e,c} - \omega_{rsi}^{c} Y_c, \tag{18}$$

where relative parts η_e and η_c of the total flux out of grain face to edge and corner bubbles, respectively, for simplicity are assumed to be equal to the relative numbers of corresponding bubbles on an edge: $\eta_e = N_{bpe}/(N_{bpe} + 1)$ and $\eta_c = 1 - \eta_e$ (where N_{bpe} is the number of edge bubbles per edge).

Eqs. (16)–(18) describe evolution of extra-granular porosity up to the moment when corresponding saturation conditions are attained. The grain face saturation by fission gas is supposed to be attained when the projected area coverage of the grain face by bubbles, $\phi = (R_f \sin\theta_f / R_s)^2$, exceeds the critical coverage $A^* = 0.5$. This is equivalent to the condition $\pi\cdot(R_f\cdot\sin\theta_f)^2 C_f = A^*\cdot 3/d_{gr}$, if the projected area coverage per unit volume is considered. The grain edge and grain corner porosity saturation takes place when these bubbles are just touching each other ($N_{bpe} l_e = L_{edge} - 2R_c$, where $L_{edge} = (\pi/6\cdot 2^{1/2})^{1/3} r_{gr}$ is an average edge length) [4].

Volume concentrations of different types of inter-granular bubbles are determined by the fuel structure:

$$C_f = \frac{N_{bpf} N_{fpgr}}{V_{gr}} = \frac{3}{d_{gr}} \frac{1}{\pi R_s^2}, \qquad C_e = \frac{N_{bpe} N_{epgr}}{V_{gr}}, \qquad C_c = \frac{N_{cpgr}}{V_{gr}},$$

where N_{bpf} is the number of face bubbles per grain face, V_{gr} is the grain volume.

Thus, at each time step determined by the evolution of the intra-granular system, Eqs. (16-18) are numerically solved by the fourth-order Runge-Kutta scheme with adaptive time step.

2.3 Model validation

There are several experimental works where microscopic behaviour of intergranular bubbles was observed directly [9, 23]. As above mentioned, in [9] the specimens were taken from UO_2 pellets irradiated in commercial BWR (burn-up: 6~28 GWd/t) at a point between the fuel rim and middle. Grain face bubble concentration and fractional coverage were examined by scanning electron microscope fractography. In addition, radii of face bubbles were also evaluated (see Figs. 1 and 3). The irradiation temperature at the location of the specimens may be roughly evaluated as 1200°C from their maximum linear heat generation rates (between 300 and 370 W/cm). The grain sizes of the fuel and irradiation rate were approximately equal to $9\ \mu m$ and $1.8\cdot 10^{19}\ m^{-3}s^{-1}$, correspondingly. During irradiation the concentration of the inter-granular bubbles increased from $\sim 1.6\cdot 10^{13}\ m^{-2}$ (at burn-up ~16 GWd/t) to $\sim 4\cdot 10^{13}\ m^{-2}$ (at burn-up ~ 23 GWd/t) and then dropped to $\sim 1.6\cdot 10^{12}\ m^{-2}$ (at burn-up ~ 28 GWd/t). Such a temporal behaviour of the bubble concentration well correlates with the assumption of [24] that the grain face bubble coarsening occurs at a late stage of irradiation leading to the reduction of the bubble concentration, however, is not considered in the present Section. This question will be specially discussed in Section 3 where coalescence of grain face bubbles under various conditions will be studied. For the sake of simplicity, in the current calculations the concentration of face bubbles was fixed at the terminal value $1.6\cdot 10^{12}\ m^{-2}$ measured in [9, 10], being in a good agreement with the prediction of Eq. (15) at 1200°C. Correspondingly, results of the model calculations are compared with the terminal values measured in [9, 10] in Table 1.

Table 1 Modelling of experiments [9, 10]

	Face bubble diameter, nm	Fractional coverage, %	Kr release, %
MFPR calculations	216	5.9	10
Experiment	229	10.1	20

It should be noted that all the data [9, 10] are quite widely scattered from grain to grain and the measured values may be considered only as estimations. For instance, fractional coverage obtained in [10] by image analysis (see Table 1, column 3) is almost two times larger than one calculated from the measured bubble mean

size and concentration: $\pi R_f^2 X_f \cdot 100\% \approx 6.6\%$, that is in a much better agreement with the model calculation ≈ 5.9%. A rather strong uncertainty in the gas release data can be clearly seen from Fig. 2.

In the other experiment [23] UO_2 fuel irradiated to a burn-up of $2\cdot10^{26}$ m^{-3} with fission rate ≈ $2.6\cdot10^{19}$ $s^{-1}m^{-3}$ was examined by transmission and scanning electron microscopy and replication metallography. In these tests gas release was not measured, however, the fission gas distribution on the grain boundaries was characterised as a function of irradiation temperature 750–1350°C.

Results of the experiments [23] modelling with the basic set of the MFPR internal parameters are presented in Table 2 containing the calculated and measured values of radii and concentrations of face bubbles.

Table 2 Modelling of experiments [23]

	Face bubble radius, μm			Face bubble concentration, m^{-2}		
	T=1023 K	T=1423 K	T=1623 K	T=1023 K	T= 1423 K	T=1623 K
MFPR calculations	0.021	0.2	0.36	$1.0\cdot10^{13}$	$3.7\cdot10^{12}$	$1.2\cdot10^{12}$
Experiment	0.03	0.3–0.5	0.5	$7.5\cdot10^{12}$	$1.2\cdot10^{12}$	$2.0\cdot10^{12}$

Taking into account a wide scattering of the experimental data, the agreement between experimental and calculation results can be considered as quite satisfactory.

After validation of the new model for the grain face bubble evolution against microscopic observations of the grain face structure in [9, 23], the MFPR module with the newly implemented model was additionally verified against the integral data for gas release and fuel swelling in the Zimmermann's tests [25]. Unrestrained specimens in these tests were subjected to irradiation at high fission rates from $3.1\cdot10^{13}$ to $1.4\cdot10^{14}$ fissions/cm^3 ·s to burn-ups from 0.4 to 12.6 % of U atoms, with mean fuel temperatures from 1250 to 2000 K.

The results of calculations with the MFPR code for conditions of the Zimmermann's experiments are presented in Fig. 4. In the tests [25] of the steady-state type, the fission gas release has been evaluated by comparison of the measured concentration of the retained fission gas and actual values of the generated gas. As one can see from Fig. 4, application of the improved model of gas transport along grain faces provides about 30% earlier beginning of fission gas release from UO_2 fuel as compared with the previous MFPR version (i.e. without consideration of diffusion transport from grain faces to edges).

Commencement of fission gas release at temperature 1250 K in [25] occurred at burn-up < 2%, that is in a good agreement with the calculated burn-up value 1.5%. As temperature increases, the difference between the two MFPR versions calculations decreases. For example, at temperature 1500 K the onset of Xe release occurs at 0.7 % burn-up in the new version and at 0.9 % burn-up in the old one. At this temperature the data presented in [25] allows an accurate determination of the fission gas release commencement at 0.6 % burn-up, which well corresponds to the calculation results with the new MFPR version.

Besides timing of gas release, the implemented model of inter-granular transport also controls fuel swelling due to grain face porosity. This phenomenon will studied in the following Sections after implementation of the face bubbles coalescence model.

In conclusion of this Section an important application of the developed grain face transport model to the MOX fuel is emphasised. In the MOX MIMAS AUC fuel irradiated in PWR rods (where the centre-line temperatures as calculated lie in the range 1000 to 1200°C) there is no evidence of inter-granular bubbles [26]. In order to explain high release values and decrease of the gas content in the U-rich matrix measured in the central part of the pellet, assumption is made in [26] that in MOX fuel, there is a strong enhancement of the kinetic of xenon migration in the grain boundaries. This assumption is based on the experiments on interdiffusion of PuO_2 in UO_2 [27] which show that the cation diffusion coefficients in grain boundary is much higher (about 2 orders of magnitude) in the presence of Pu. As xenon diffusion is related to cation diffusion, it was assumed a similar evolution of the Xe diffusion coefficients.

For modelling of the MOX fuel irradiated in PWR rods in which there is no evidence of inter-granular bubbles despite fission gas release is relatively high, the new model for gas transport on grain boundaries becomes especially important. This model allows explanation of gas release without interconnection of bubbles (observed in the above described tests with UO_2 fuel [9, 10]), and thus, after certain modifications can be applied to the MOX fuel.

3 Model for grain face porosity evolution

3.1 Analysis of experimental observations

As above described, microscopic behaviour of inter-granular bubbles was observed in [9, 10], either under steady state irradiation, or under post-irradiation annealing conditions. More detailed experimental study of the bubble growth and coalescence kinetics under annealing conditions was carried out in [28]. In the tests [28] the inter-granular swelling for similar base-irradiated samples, was measured at various annealing times along with observations of the grain face microstructure evolution. In these experiments unstressed samples of uranium dioxide taken from the pressurised water reactor fuel after two normal operating cycles, i.e., with burn-up of 25 GWd/tU, were subjected to thermal treatment in a laboratory furnace at temperatures between 1130 and 1715°C for duration between 5 min and 10 h. During irradiation stage fuel core temperature did not exceed 1100°C. The variation of the quantity of fission gas released over time was measured at each temperature. The samples were also subjected to a series of isothermal swelling measurements. Their comparison provides information on the inter-granular, intra-granular, open and closed porosity.

Experimental results of interest obtained in this work are presented in Figs. 5 and 6. From these data the following conclusions can be derived:

- Kinetics of inter-granular swelling consist of two distinct stages: a rapid swelling phase with the duration time of about several tens of minutes, and the second phase when the process slows down;
- As the annealing temperature grows, the concentration of face bubbles decreases and their radii increase;
- At the highest annealing temperature (1715°C) the inter-granular swelling is saturated after 5 hours of treatment;

Therefore, quantitative analysis of inter-granular micrographs shows a decrease in the number of face bubbles per unit grain boundary square and an increase in the bubble size, with increase of treatment time and temperature.

3.2 Model development and validation

In order to explain the observed kinetics of grain face swelling under annealing conditions, the authors of [28] assumed that during heat treatment face bubbles become mobile and migrate at random on grain surface, and then coalesce. The theory of grain face bubble coalescence was developed in [29] where kinetics of the bubble system evolution with time was calculated. Apparently lacking these theoretical results, the authors [28] attempted their own approach to the same problem. Despite that their new calculations were rather cumbersome and overcomplicated, Zacharie et al. managed to reproduce the main kinetic dependencies of bubble number and size on time in a good agreement with the general theory [29]. As a result, an explicit equation for inter-granular swelling as function of treatment time and temperature was derived in their work. This equation provides a good description of the measured swelling values after fitting of its parameters to the experimental data.

In this Section the coalescence of face bubbles due to their random migration is considered on the base of the general theory [29], and the main analytical results of [28] are deduced in a more straightforward and simple way. This allows elimination of some inconsistencies in the approach of [28] and improvement of the model predictions against additional experimental observations [9, 10] of grain face bubbles behaviour under similar annealing conditions. Moreover, more general approach proposed in the current paper allows an extension of the new model to more general conditions (e.g. steady irradiation or transient) than considered in the simplified approach of [28] which is valid only for specific annealing conditions of these tests.

In analogy with the description of intra-granular bubbles, the general equation for the kinetics of surface concentration of bubbles on the grain faces can be written in the following form:

$$\frac{dX_f}{dt} = \omega_{nuc} X_g^2 - \omega_{cls} X_f^2, \tag{19}$$

where ω_{nuc} is frequency of bubble nucleation, ω_{cls} is frequency of coalescence of bubbles, X_g is surface concentration of atoms on the grain faces. The first term in the r.h.s. of Eq. (19) describes nucleation of new bubbles on grain faces. Under steady state irradiation conditions (after some initial, relatively short time interval), concentration of gas atoms on grain surfaces is close to some quasi-equilibrium value X_g^{eq} that can smoothly vary with time (compare with Eq. (9)). This concentration of grain surface atoms determines quasi-equilibrium concentration of face bubbles and, as follows from Eq. (19), under stationary conditions:

$$X_f^{eq} = \sqrt{\frac{\omega_{nuc}}{\omega_{cls}}} X_g^{eq}, \tag{20}$$

This concentration of face bubbles was independently measured in different experimental works and approximated in the MFPR code by Eq. (15). For small deviations from the equilibrium concentration, one can substitute Eq. (20) into Eq. (19) and obtain:

$$\frac{dX_f}{dt} = \omega_{cls}\left[(X_f^{eq})^2 - X_f^2\right], \tag{21}$$

After cessation of fuel irradiation, surface concentration of atoms considerably drops due to their rapid sinking into bubbles, and nucleation term in Eq. (21) tends to zero:

$$\frac{dX_f}{dt} = -\omega_{cls} X_f^2. \tag{22}$$

Coalescence frequency of bubbles randomly moving on a surface can be represented by the formula derived in [29]:

$$\omega_{cls} = \frac{8\pi D_b}{\ln(\frac{D_b}{2R_f^2}\tau_0)} \approx 8\pi\alpha D_b, \tag{23}$$

where τ_0 is the characteristic time of two-fold increase of the mean bubble radius R_f. Being a weak function of its argument (and thus, of D_b), logarithm can be approximated by a constant value, i.e. $\alpha \approx$ const.

It is worth to note here for comparison that for the intra-granular bubbles the coalescence frequency is additionally proportional to the bubble radius: $\omega_{cls} \sim R_b D_b$, thus, the kinetics of their evolution might be significantly different.

Bubble diffusion coefficient D_b is generally represented in the form:

$$D_b = D_0 \exp(-\frac{Q}{RT})\frac{1}{R_f^q}, \tag{24}$$

where exponent q depends on the dominating microscopic mechanism of bubble migration. In the case of mass transport on bubble surface $q = 4$, i.e. $D_b \sim (1/R_f)^4$, whereas for volume diffusion mechanism $q = 3$ and $D_b \sim (1/R_f)^3$. By fitting procedure of the measured and calculated results, the authors [28] evaluated the main parameters in Eq. (24) as Q = 310 kJ/mol and q = 3.4. To their opinion, the latter value corresponds to the mixed mechanism of bubble movement on grain surface.

After attainment of grain face saturation coverage, face bubble concentration additionally obeys the limiting coverage condition:

$$\pi\left[R_f(t)\sin\theta_f\right]^2 X_f(t) = A^*. \tag{25}$$

Under isothermal annealing conditions solution of coupled Eqs. (22) and (25) has an asymptotic form:

$$R_f = \left[A^* 4(q+2)\alpha D_0 \exp(-\frac{Q}{RT})t\right]^{\frac{1}{q+2}}, \tag{26}$$

which practically coincides in form with that found in [28]. However, instead of the usual saturation condition, Eq. (25) (i.e. coverage of the grain surface by bubbles is fixed after saturation), the authors of [28] used an assumption that the number of fission gas atoms trapped at the grain boundary surface remains constant as coalescence proceeds:

$$N_f X_f = M \text{ or } R_f^2 X_f = \frac{MkT}{2\gamma_f}, \tag{27}$$

where γ is UO_2 surface tension. Being formally similar to Eq. (25), , the r.h.s. of Eq. (27) additionally depends on temperature (instead of constant value $A^* \approx 0.5$ in Eq. (25)), which results in a strong dependence of grain face coverage on temperature. This prediction contradicts to experimental observations, e.g. of [9, 10], where the surface coverage after heat treatment always attained the limiting value of 0.4-0.5 being roughly independent of the heating conditions and specimen burn-up.

Another improvement of the approach proposed in [28] is inclusion of edge and corner porosity into consideration. Indeed, the authors of [28] attributed inter-granular swelling solely to face bubbles, however, it is well known that edge and corner porosity may contribute to overall swelling as much as face bubbles or even more.

An important advantage of the new approach based on kinetic Eqs. (19) or (21), is that one can extend the model for bubble coalescence to more general (e.g. steady irradiation or transient) conditions, whereas Eq. (26) derived in [28] is valid only for specific conditions of annealing tests.

The new model for relaxation of face bubbles based on Eqs. (21)–(25), was implemented into the MFPR code. Activation energy of face bubble diffusion and dependence of D_b on bubble radius was accepted as found in [28]. Pre-exponential factor in Eq. (24) was determined by fitting of experimental data [28] and MFPR results and appeared to be

$$\alpha D_0 = 2.6 \cdot 10^{-4-8q} \approx 1.3 \cdot 10^{-31} \ \ [\mathrm{m^2/s}]. \tag{28}$$

It might be assumed that owing to the above mentioned (in Section 2.1.2) extremely high diffusivity of gas atoms on grain faces ($D_f / D_g \sim 10^5$), bubble diffusion coefficient can be also much larger on grain faces than in the grain bulk (owing to enhanced transport of gas atoms along the grain face). Justification of this assumption requires an additional consideration of the problem that could explain relatively high values of bubble diffusivity (in comparison with the bulk values) determined by Eqs. (24) and (28).

A comparison of measured in [28] mean linear bubble concentrations with the MFPR predictions at different temperatures is presented in Fig. 7. So, the observed evolution of bubbles on grain surfaces is reproduced by MFPR with the new inter-granular bubble coalescence model within 30% of accuracy.

Swelling values calculated by the model with the above presented parameters are compared with the measured in [28] data in Fig. 8. As one can see from this figure, a slow phase of swelling evolution is quite well reproduced by the MFPR code, however, at low temperatures absolute values of calculated swelling are higher than the measured ones. Analysis of swelling components calculated by the code reveals that the main contribution to the porosity at these temperatures is due to edge and corner bubbles. Thus, for more adequate description of fuel swelling in this temperature range a further improvement of the edge porosity model is recommended.

The model predictions for fuel swelling under steady irradiation conditions of the Zimmermann's tests [25] are also in a satisfactory agreement with the measurements, Fig. 9.

4 Conclusions

The advanced model for the grain face transport based on the self-consistent consideration of diffusion and resolution processes in the grain and grain faces, is developed. An important role of grain boundary diffusion of gas atoms to edges before interlinking of inter-granular bubbles, is outlined.

Implementation in the MFPR code of the new model and numerical treatment of various available data on gas release from irradiated fuel, show a satisfactory agreement of the code predictions with measurements. Calculations of the inter-granular bubbles growth kinetics are also in a fair agreement with the grain face microstructure observations.

As a result, an important conclusion is derived that at low irradiation temperatures ($\leq 1200^\circ$C) gas release commences significantly earlier than predicted by the standard approach. This leads to important consequences with respect to the gas release predictions for the real fuel pellets, and especially for the MOX fuel.

The coalescence of face bubbles due to their random migration is considered as the main mechanism of grain face bubbles relaxation. The model of this phenomenon proposed in [28] for annealing conditions is refined and extended to the general case of fuel operation conditions (e.g. steady-state irradiation and temperature transients).

Validation of the new model against the fuel swelling measurements [25, 28] allows a significant improvement in the code predictions also in this area.

Acknowledgements

The authors thank Drs. V. Ozrin and V. Tarasov (IBRAE) for valuable discussions and comments. This work was supported by IPSN, Cadarache (France) under the Contract No. 4000 A 109310 on the mechanistic code MFPR development; the personal support and collaboration of Drs. R. Dubourg, P. Giordano and M. Kissane (IPSN) are highly appreciated.

References

1. M.S. Veshchunov, J. Nucl. Mater., 277 (2000) 67.
2. A.V. Berdyshev, R.R. Galimov, V.D. Ozrin, A.V. Palagin, V.E. Shestak, M.S. Veshchunov, "MFPR version 1.1 revision 1 module. User manual", - Note Technique SEMAR 99/55, IPSN-CEA, Cadarache, France, 1999.
3. M.S. Veshchunov, A.V. Berdyshev, V.I. Tarasov, "Development of Fission Gas Bubble Models for UO_2 Fuel in Framework of MFPR Code", Preprint IBRAE-2000-08, Moscow, 2000.
4. R.J. White, M.O. Tucker, J. Nucl. Mater., 118 (1983) 1.
5. W. Beere, G.L. Reynolds, J. Nucl. Mater., 47 (1973) 51.
6. C.C. Dollins, F.A. Nichols, J. Nucl. Mater., 91 (1976) 143.
7. T.J. Heames, D.A. Williams, N.E. Bixler, A.J. Grimley, C.J. Wheatley, N.A. Johns, P. Domogala, L.W Dickson, C.A. Alexande, I. Osborn-Lee, S. Zawadzki, J. Rest, A. Mason, R.Y. Lee, "VICTORIA: A Mechanistic Model of Radionuclide Behaviour in the Reactor Coolant System under Severe Accident Conditions",- NUREG/CR-5545, 1992.
8. I.J. Hastings, J. Nucl. Mater., 54 (1974) 138.
9. K. Une, S. Kashibe, J. Nucl. Sci. Technol., 27 (1990) 1002.
10. S. Kashibe, K. Une, J. Nucl. Sci. Technol., 28 (1991) 1090.
11. J.A. Turnbull, J. Nucl. Mater., 50 (1974) 62.
12. J.A. Turnbull, M.O. Tucker, Philos. Mag., 30 (1974) 47.
13. M.H. Wood, J. Nucl. Mater., 119 (1983) 67.
14. J.R. Matthews, M.H. Wood, J. Nucl. Mater., 91 (1980) 241.
15. P. Van Uffelen, "Assessing the contribution of grain boundary diffusion to fission gas release in nuclear fuel", Enlarged Halden Programme Group Meeting, Loen (Norway), 1999.
16. M.V. Speight, Nucl. Sci. Engrg., 37 (1969) 180.
17. P. Van Uffelen, "Development of a new fission gas release and fuel swelling model", Enlarged Halden Programme Group Meeting, Lillehammer (Norway), 1998, HPR-349.
18. G.B. Alcock, R.J. Hawkins, A.W.D. Hills, P. McNamara, Paper SM-66/36, IAEA, Symp. Thermodynamics, Vienna, 1965, p. 57.
19. M.O. Tucker, J. Nucl. Mater., 89 (1979) 199.
20. P.J. Clemm, J.C. Fisher, Acta Metall., 3(1955)70.
21. R.S. Nelson, J. Nucl. Mater., 31 (1969) 153.
22. J.A. Turnbull, R.M. Cornell, J. Nucl. Mater. 41(1971)156.
23. S.R. Pati, M.J. Dapt, D.R. O'Boyle, J. Nucl. Mater., 50 (1974) 227.
24. C.T. Walker, P. Knappik, M. Mogensen, J. Nucl. Mater., 160 (1988) 10.
25. H. Zimmermann, J. Nucl. Mater., 75 (1978) 154.
26. Y. Guerin, J. Noirot, D. Lispaux, C. Struzik, P. Garcia, P. Blainpain, G. Chigne, "Microstructure evolution and in-reactor behaviour of MOX fuel", Proc. Int. Top. Meet. LWR Fuel Performance, April 10-13, 200, Park City, Utah, USA, pp. 706-719.
27. S. Mendez, "Etude de l'interdiffusion U-Pu applique au combustible MOX", Thesis Universite Aix-Marseille, 1995.
28. I. Zacharie, S. Lansiart, P. Combette, M. Trotabas, M. Coster, M. Groos, J. Nucl. Mater., 255(1998)85-91.
29. Ya.E. Geguzin and M.A. Krivoglaz, "The Movement of Microscopic Inclusions in Solid State" (Metallurgiya, Moscow, 1971, in Russian).

Figures

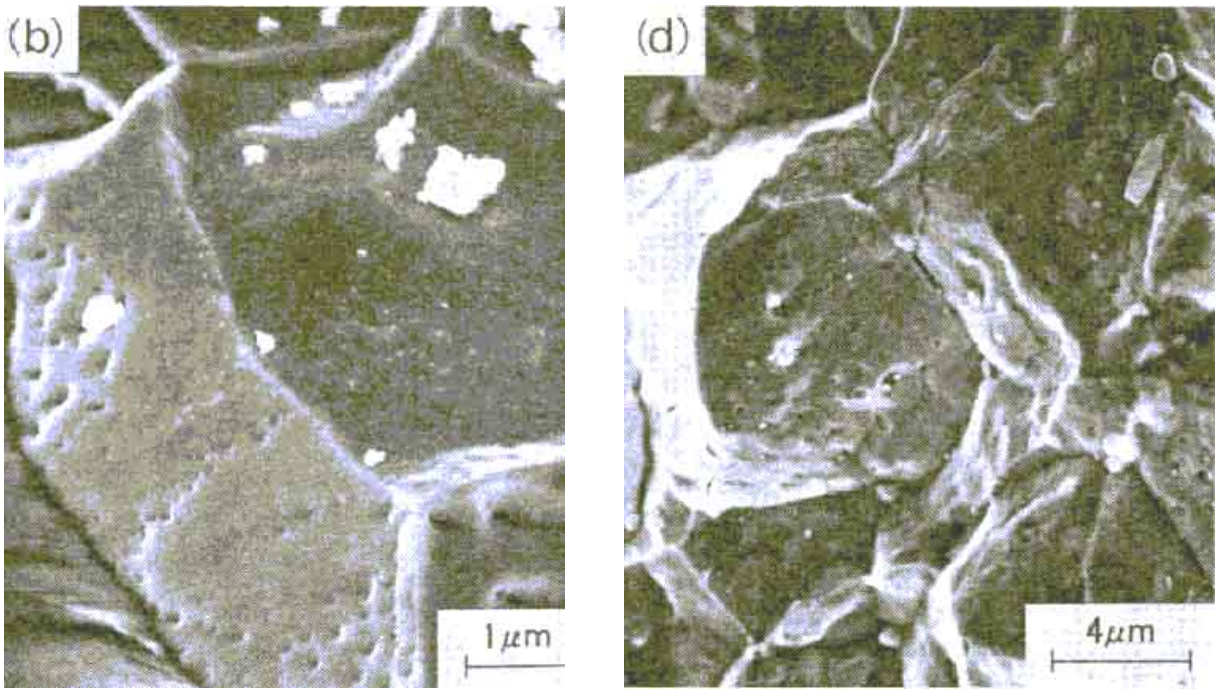

2 cycle specimen *4 cycle specimen*

Fig. 1. Scanning electron micrographs of fracture surface of as-irradiated specimens (from [9]).

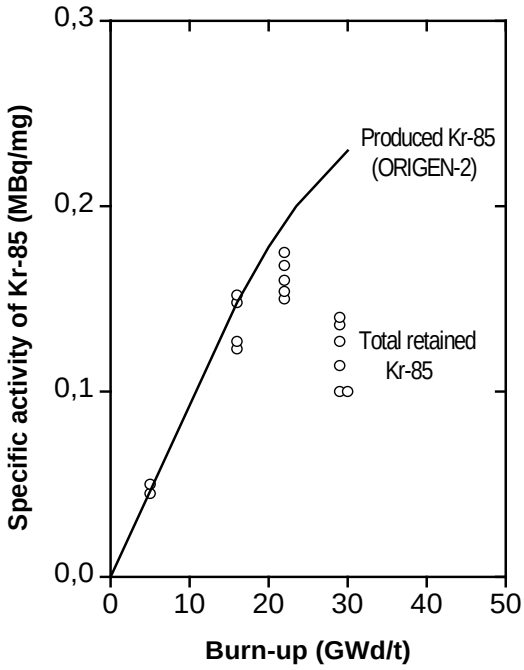

Fig. 2. ^{85}Kr concentrations in UO_2 as a function of burn-up (from [9]).

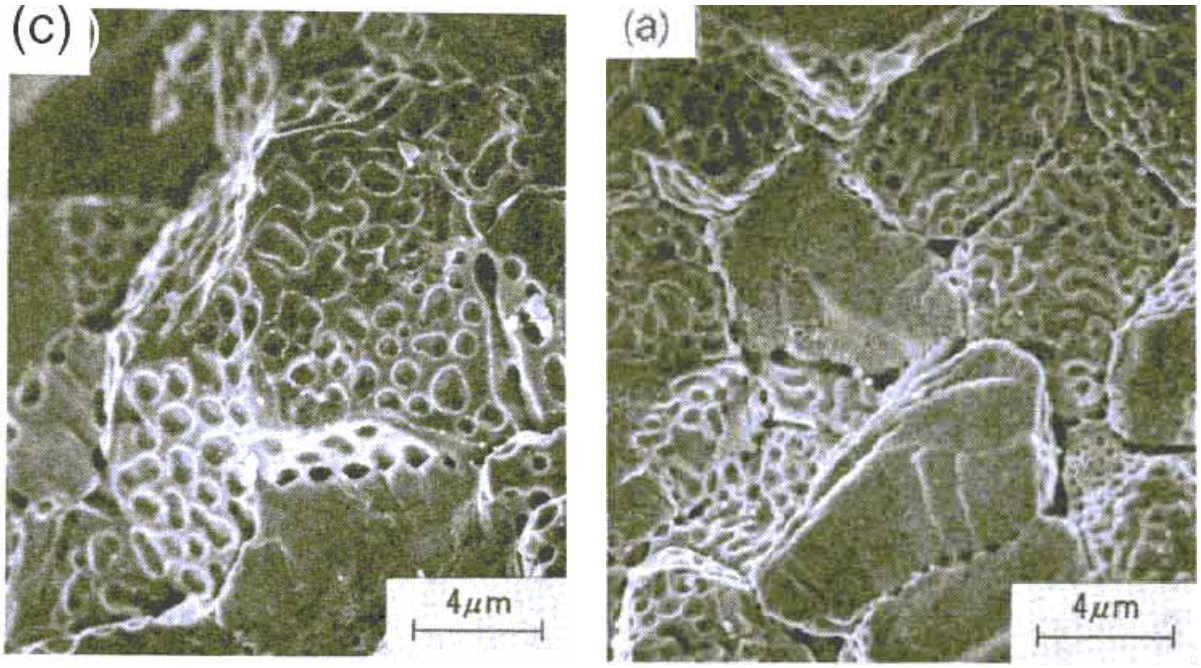

2 cycle specimen *4 cycle specimen*

Fig. 3. Scanning electron micrographs of fracture surface of post-irradiated specimens heated up to 1800 ℃ (from [9]).

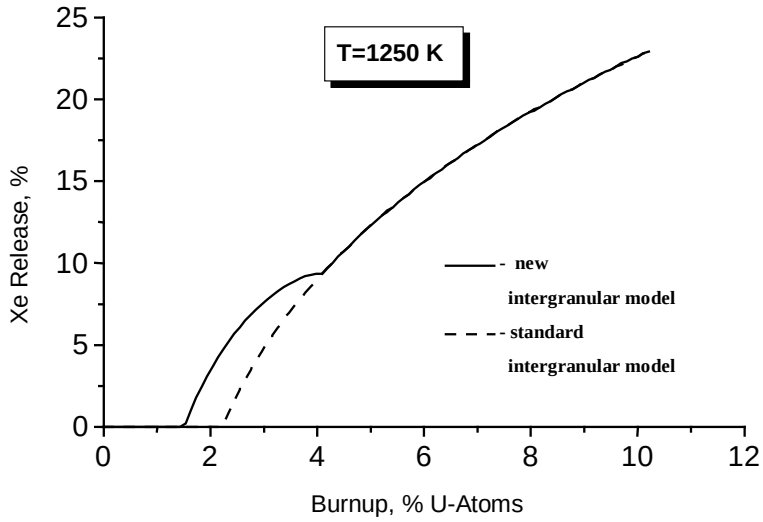

Fig. 4. Xe release from UO_2 as a function of burn-up for conditions of Zimmermann's tests [25] at T = 1250 K, calculated by two inter-granular model.

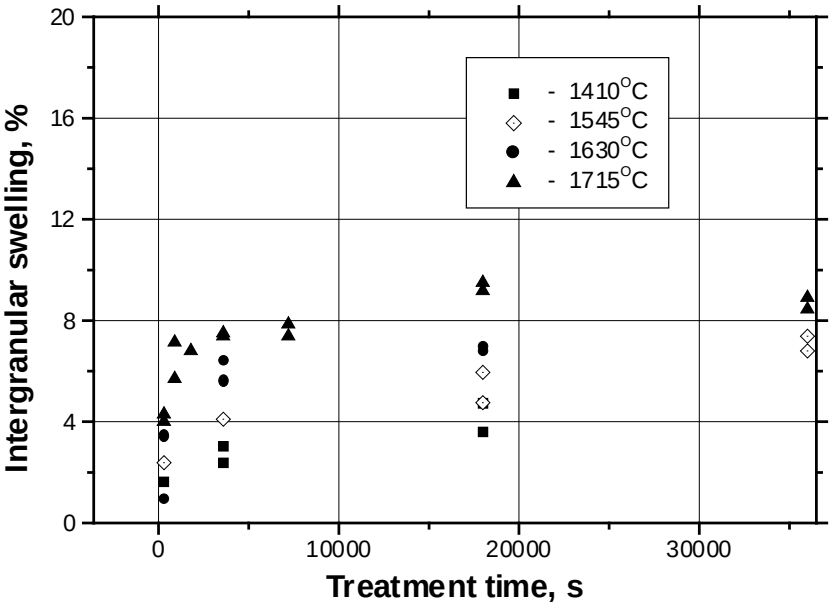

Fig. 5. *Inter-granular swelling as a function of treatment time at different temperatures measured in [28].*

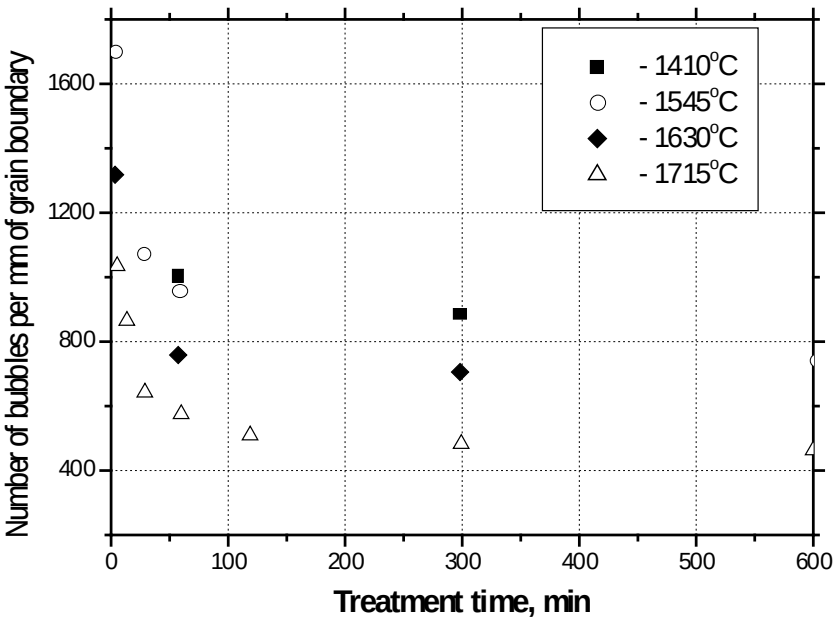

Fig. 6. *Number of bubbles per millimetre of grain boundary as a function of treatment time at different temperatures measured in [28].*

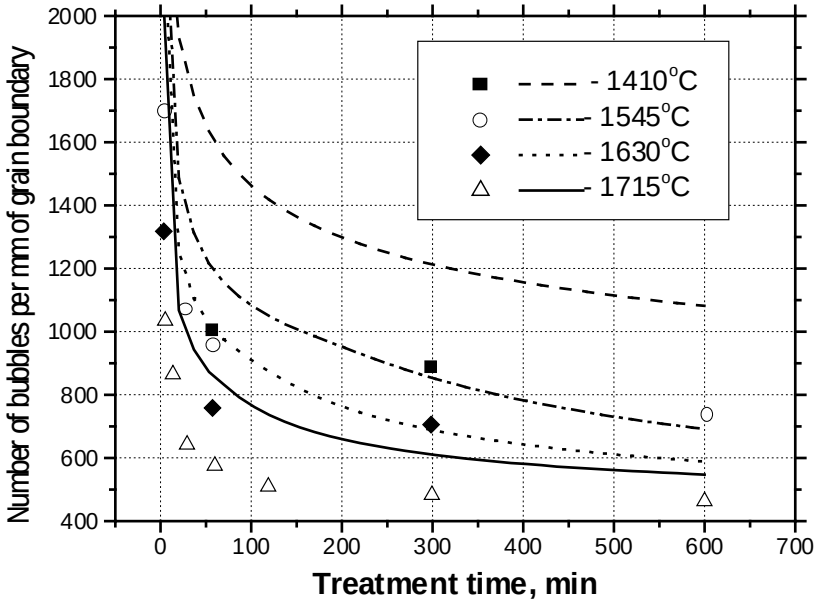

Fig. 7. *Number of face bubbles per millimetre of grain boundary as a function of annealing time at different temperatures. Curves represent calculations, dots are experimental data [28].*

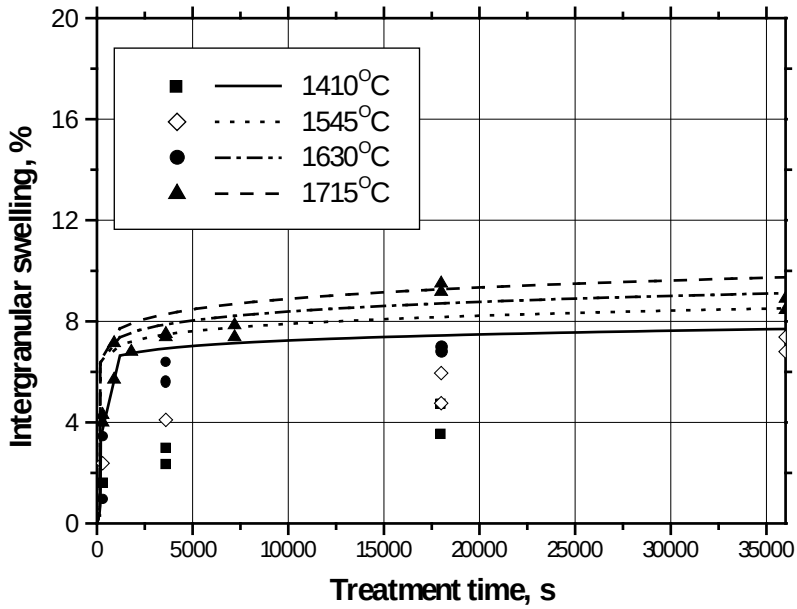

Fig. 8. *Inter-granular swelling as a function of treatment time at different temperatures. Curves represent calculations, dots are experimental data measured in [28].*

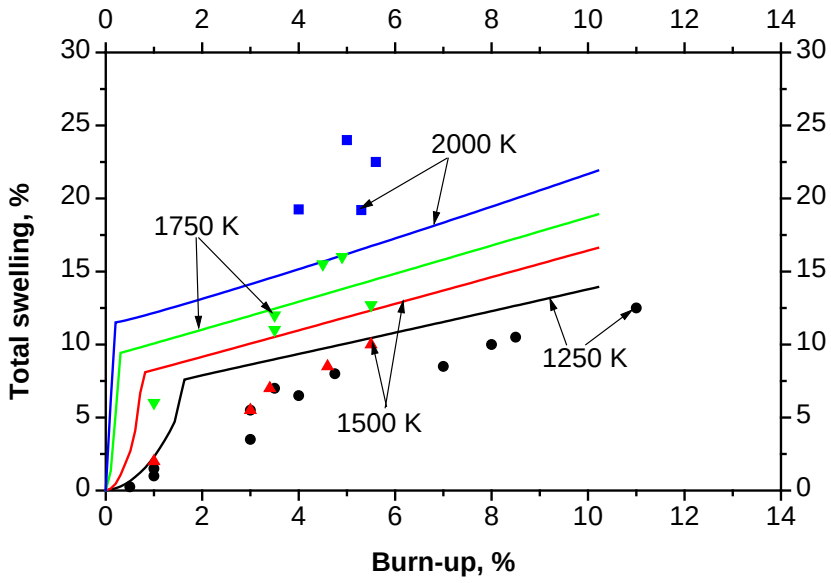

Fig. 9. *Swelling under steady irradiation conditions of Zimmermann's test, calculated by the new model with account for contribution of solid fission products into total swelling. Data points are from [25].*